SF2A 2019
P. Di Matteo, O. Creevey, A. Crida, G. Kordopatis, J. Malzac, J.-B. Marquette, M. N'Diaye, O. Venot (eds)

COSMOS/GOODS-S FIELDS SPECTRO-PHOTOMETRIC ANALYSIS AND THE MOONS FUTURE PERSPECTIVES IN SED FITTING STUDIES

J. A. Villa-Vélez[1], V. Buat[1], D. Burgarella[1], M. Rodrigues[2], M. Puech[3] and H. Flores[3]

Abstract. Soon, the MOONS spectrograph will provide forefront scientific spectroscopic data enriching the current panorama of chemical composition and evolution of galaxies. Currently, multi-wavelength observations are vital to performing SED fitting analysis to understand the star-forming history of our universe and how dust attenuation affects their derivation. However, most of the analysis is carried out using only photometric data. Coupling spectroscopy and photometry gives us a more powerful tool to study the implication of dust attenuation and undergoing physics. We target objects in the COSMOS and GOODS-S fields using current spectroscopic data from the 3D-HST (i.e. H_α+[NII], H_β and [OIII] emission lines) and available photometric data to perform SED fitting using the CIGALE-code. We discuss how faithfully each emission line can be fit with CIGALE and how different dust attenuation recipes can affect the results. This work will serve as an important basis for future studies when MOONS data comes into play and we need to combine photo-spectroscopic data.

Keywords: catalogs, galaxies: high-redshift, galaxies: emission lines, ISM: dust, extinction,

1 Introduction

Deriving reliable properties of galaxies is paramount to understand the current theory of formation and evolution of galaxies. Spectral energy distribution (SED) fitting is widely used to achieve these goals. This method relies only on the analysis of photometric data using bands from the UV-to the-IR. Recently, in different SED fitting codes as CIGALE spectroscopic information as emission line fluxes or equivalent widths can be analyzed altogether with the photometric data providing a more accurate picture on the determination of stellar masses, star formation histories and the amount of dust attenuation for a given emission line.

Understanding how dust affects the emission lines allows us to determine the amount of attenuation which is vital to accurately measure the physical properties of galaxies and the possible correlations with other parameters. The SED fitting process allows us to quantify the amount of attenuation for a given emission line giving us a powerful tool for correcting the derived physical properties but also calibrating, for example, the star-formation estimates.

Traditionally the H_α line is used as a good tracer of star-formation. Even so, at high-redshift, this line is not observable and other emission lines must be implemented. In the past, [OII] has been widely studied (Kewley et al. 2004; Talia et al. 2015) and [OIII] has been recently proposed as a good tracer of SFRs in star-forming galaxies (Steidel et al. 2014; Suzuki et al. 2016; Khostovan et al. 2016). Therefore, we need to understand the correlation of [OIII] line with other physical parameters either from models or well-defined, and representative samples. Our aim, in this case, is encouraged by the previous works mentioned above to understand how current available [OIII] flux density data can be used to study its correlation with star-formation derived from SED fitting and propose a calibration for star-forming galaxies. We also aim to investigate how the different attenuation laws affect the reproducibility of [OIII]. Different authors (see: Corre et al. 2018; Buat et al. 2018; Malek et al. 2019; Buat et al. 2019) have shown how the attenuation law affects different parts of the spectrum and some modifications to current recipes have been proposed. Here a brief exercise fitting COSMOS and GOODS-S data using CIGALE and the Calzetti et al. (2000) and Charlot & Fall (2000) recipes are presented.

[1] Aix Marseille Université, CNRS, LAM (Laboratoire d'Astrophysique de Marseille) UMR 7326, 13388, Marseille, France
[2] Astrophysics, Department of Physics, Denys Wilkinson Building, Keble Road, Oxford OX1 3RH, UK
[3] GEPI, Observatoire de Paris, PSL University, CNRS, 5 Place Jules Janssen, F-92190 Meudon, France

2 Sample selection

We focus on two different fields. The COSMOS field which is centered at α(J2000) = $10^h0^m27.9^s$ and δ(J2000) = $0^h8^m50.3^s$ (Scoville et al. 2007) and the GOODS-S field centered at α(J2000) = $03^h32^m30^s$ and δ(J2000) = $-27^d48^m20^s$ (Guo et al. 2013). For COSMOS, we start with the multi-wavelength catalog of Laigle et al. (2016), COSMOS2015, which contains *UBVrizyJHK$_s$* photometry from CFHT megacam and wircam, SUBARU suprime and HSC, and UKIRT WFC respectively. For the infra-red range we have Spitzer IRAC *3.6, 4.5, 5.8, and 8.0 μm* data obtained from Laigle et al. (2016) and cross-matched to HELP-project Spitzer MIPS *24 μm*, Herschel PACS *100, and 160 μm*, and Herschel SPIRE *250, 350, 500 μm*. The GALEX NUV data was obtained also from the HELP-project. Emission line density fluxes and spectroscopic redshift comes from the 3D-HST catalog of the v4.1.5 release with WFC3 G141 grism spectroscopy (Brammer et al. 2012; Momcheva et al. 2016). We kept density fluxes for H$_\alpha$+[NII], H$_\beta$, and [OIII] because they are prominent lines, really well-studied and important for the determination of dust attenuation, stellar mass, metallicity among other properties.

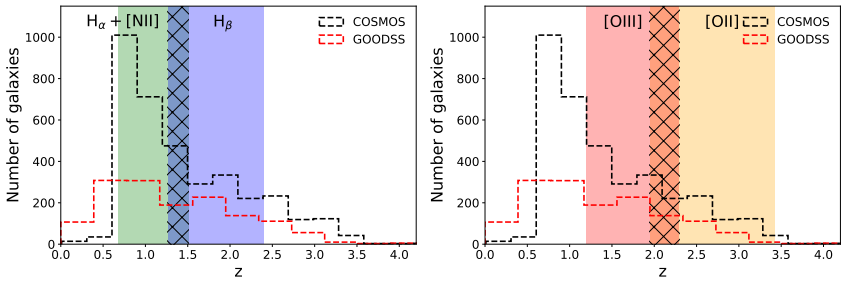

Fig. 1. Redshift distribution of COSMOS (black dashed line) and GOODS-S (red dashed line) final samples. **Left:** The H$_\alpha$+[NII] and H$_\beta$ expected coverage of the WFC3 G141 grism are shown in green and purple respectively. **Right:** Same as in left panel but using [OII] and [OIII] emission lines. We cover an important redshift range with several emission lines.

On the other hand for GOODS-S field we use the CANDELS GOODS-S multi-wavelength catalog (Guo et al. 2013, and references therein). The photometric data corresponds to *U-VIMOS*, and *F435W, F606W, F775W, F814W, F850LP* HST/ACS, *F098M* HST/WFC3, and *F105W, F125W, F160W* CANDELS+HUDF09, ISAAC-K$_s$, and Spitzer IRAC *3.6, 4.5, 5.8, and 8.0 μm*. We crossmatch the PACS *70, 100, and 160 μm*, and Herschel SPIRE *250, 350, 500 μm* from the PEP-catalog (Lutz et al. 2011; Wang in prep.). Spectroscopic redshift and H$_\alpha$+[NII], H$_\beta$, and [OIII] density fluxes are also obtained from the 3D-HST catalog. The GALEX NUV data used comes from the Great Observatories Origins Deep Survey: far-infrared imaging with Herschel" (GOODS-Herschel, Elbaz et al. (2011)) survey.

The final samples are crossmatched to X-ray CHANDRA observations for COSMOS (Civano et al. 2016; Marchesi et al. 2016) and GOODS-S Dickinson et al. (2003). Objects detected in X-ray were rejected due to potential active galactic nuclei. Besides, objects for which the GALEX NUV measurements fall below the Lyman limit (912$\AA$) are kept but the NUV information is neglected because these measurements are not reliable. For the WF3 G141 grism this corresponds to galaxies below z< 0.856. The distribution of the final sample for both fields is shown in Fig. 1 as a function of redshift along with the WFC3 G141 emission line coverage.

3 CIGALE SED fitting: H$_\alpha$+[NII], H$_\beta$ and [OIII]-emission lines

The final samples for COSMOS and GOODS-S are fit using CIGALE-code which allows fitting simultaneously photometry and spectroscopy. Currently, in CIGALE there are two attenuation recipes implemented (e.g. Starburst-Modified and CF00-Modified). The former uses the well-known attenuation curve of Calzetti et al. (2000) but extended between the Lyman break and 150nm as a basis and a power law as a function of the wavelength which allows the variation of the slope. A Lorentzian-like Drude profile allows adding the UV-bump in Eq. 3.1. This law is defined for the continuum and the emission lines are only dimmed by the Milky Way extinction curve. A more flexible approach allows to use an updated version of the Milky Way curve and also those of the Small and Large Magellanic Clouds Boquien et al. (2019). On the other hand, the latest is based on the Charlot & Fall (2000) recipe where young and old stellar populations are embedded in different environments thus experiencing different attenuation. The light emitted by young stars inside the birth clouds

is attenuated by the birth cloud and the ISM. The old stars are only attenuated by the ISM where they are embedded in. Here, old stands for stellar age > 10Myr in Eq. 3.2.

$$A(\lambda) \quad = \quad E(B-V)_{star}\ k'(\lambda)\ \left(\frac{\lambda}{\lambda_v}\right)^{\delta} \tag{3.1}$$

$$A(\lambda) = \begin{cases} A_V^{BC}(\lambda/\lambda_v)^{n^{BC}} & \text{if stellar age} < 10\text{Myr} \\ \\ A_V^{ISM}(\lambda/\lambda_v)^{n^{ISM}} & \text{if stellar age} > 10\text{Myr} \end{cases} \tag{3.2}$$

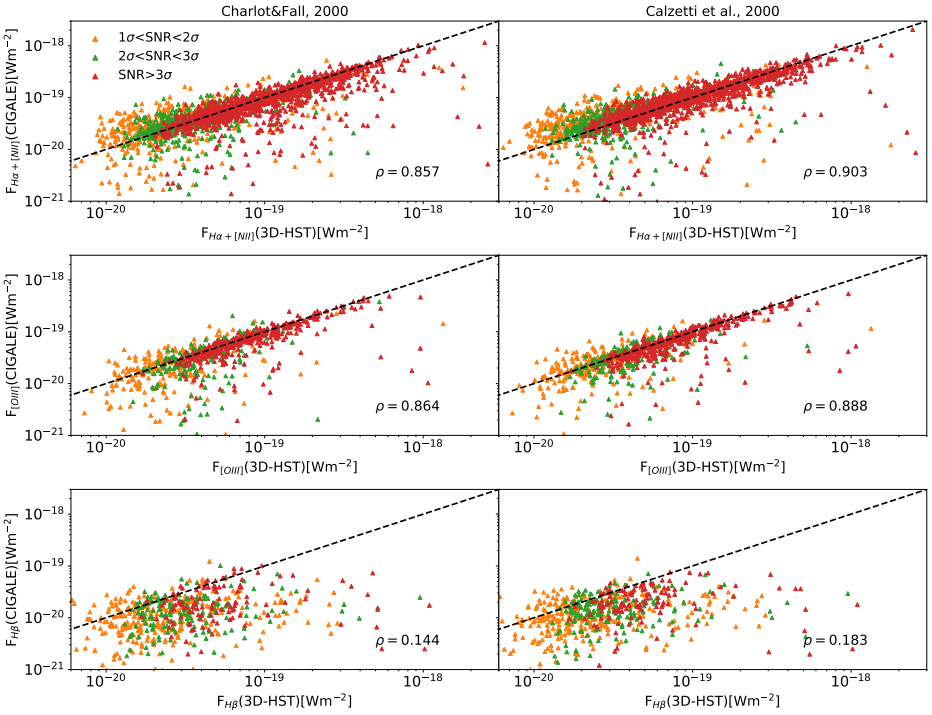

Fig. 2. H_α+[NII], H_β and [OIII] density fluxes vs CIGALE fits for COSMOS using Charlot & Fall (2000) and Calzetti et al. (2000) recipes. In all panels, the color-code stands for the signal-to-noise ratio. The black line represents the 1:1 relation and ρ corresponds to the Pearson correlation factor.

We checked and analyzed that emission line fitting works for the most simple and well-known cases we fit both the COSMOS and GOODS-S data using the traditional Calzetti et al. (2000) and Charlot & Fall (2000) (hereby: C00 and CF00 respectively) laws which can be easily retrieved from the modified laws in CIGALE. This means, that in Eq. 3.1 the reduction factor ($E(B\text{-}V)_{star}/E(B\text{-}V)_{lines}$) is set to 0.44, and the slope δ of the power-law is zero. On the other hand, in Eq. 3.2, we fix the power-law slopes for the birth cloud n^{BC} and the ISM n^{ISM} to -0.7 and the ratio of the attenuation in the V band experienced by old and young stars to 0.3. In Fig. 2 the results for H_α+[NII], H_β, and [OIII] are shown for the COSMOS samples as fitted by using the C00 and CF00 attenuation laws. Same results are obtained for the GOODS-S field but only COSMOS is presented for clarity.

For the H_β line it is evident that both recipes fail to faithfully reproduce the observed density fluxes. CIGALE does not fit this line independently of the data quality which raises the question if the current attenuation laws need to be modified or any other parameters inside the physical models need to be changed to reproduce the line. However, we need to be cautious because the vast majority are below the 3σ threshold, fluxes are really small, and measuring the line is quite difficult. As can be seen in Fig. 2 the difference between the CF00 and C00 fitting is not statistically significant as shown by the Pearson correlation coefficients.

The next step consists in using the more flexible modified recipes implemented in CIGALE which allow us to vary the slopes and explore a wider range of scenarios aiming to reduce the scatter. A small test sample confirms that the scatter can be improved but no real change in the prediction of the H_β line. This also ameliorates the small offset present in the H_α fit when using CF00 as compared to C00. Both H_α+[NII] and [OIII] emission are fairly well reproduced by our fitting analysis using the two different recipes. The fact that the [OIII] line is well reproduced is very encouraging for this work because we aim to calibrate it in terms of star-formation as has been done before with the H_α line. Although the number of objects is a bit less for the [OIII] sample compared to the H_α one, we observe that the sample is less scattered. A good fit for our samples is crucial because all the physical properties derived from the SED fitting analysis as the SFR, stellar masses, metallicities, among others will strongly depend on how well we can reproduce the photometric and spectroscopic data at the same time.

4 MOONS perspectives

The Multi-Object Optical and Near-infrared Spectrograph (MOONS) will be placed on the Nasmyth platform of one of the VLT telescopes. The first light is expected around 2021. The instrument is composed of two different spectrographs both equipped with slits containing 32 slitlets, and 16 fibers. Only 1001 fibers out of 1024 are connected to the FPUs to allow for some flexibility in matching the slitlets. The instrument is planned to have a wavelength coverage between 0.8μm and 1.8μm, and to work in three different resolution modes (R$\sim$4,000-6,000 in the entire wavelength range, R$\sim$8,000 around the CaII triplet, and R$\sim$20,000 in the J-band and H-band) which makes it a valuable instrument to explore and study emission line features which are usually shifted to the IR-range and highly affected by dust attenuation Cirasuolo et al. (2012).

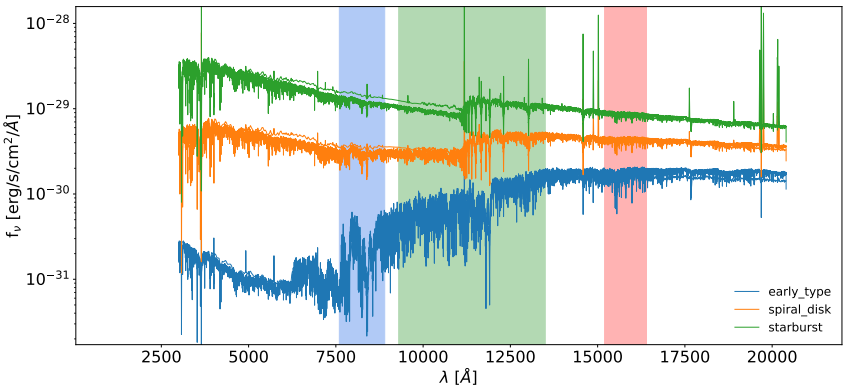

Fig. 3. High-resolution spectra for a different type of galaxies modeled using CIGALE. Each spectrum corresponds to an early-type, spiral or starburst type of galaxy. Several samples were generated varying the amount of attenuation. The vertical bands correspond to the three bands wavelength covered by MOONS.

As part of the End2End simulation for MOONS, we implemented high-resolution SSPs ELODIE-based models into CIGALE as presented by Maraston & Strömbäck (2011) (MS11). The Bruzual & Charlot (2003) (BC03) high-resolution models already implemented in CIGALE may not be sufficient to analyze the continuum as we want to degrade the spectra through the simulation. In Fig. 3 a small sample covering the three types of galaxies is presented. Each spectrum was obtained with CIGALE using the MS11-HR models for the continuum and BC03-HR models for the emission lines in a restricted wavelength range imposed by the MS11 models. Implementing emission lines along with high-resolution MS11 models will be addressed in future work. These samples represent the first attempt to test the MOONS ETC and provide some training data set for the extragalactic and redshift determination teams.

References

Boquien, M., Burgarella, D., Roehlly, Y., et al. 2019, A&A, 622, A103
Brammer, G. B., van Dokkum, P. G., Franx, M., et al. 2012, ApJS, 200, 13
Bruzual, G. & Charlot, S. 2003, MNRAS, 344, 1000

Buat, V., Corre, et al. 2019, arXiv e-prints, arXiv:1902.09435
Buat, V., Boquien, M., Małek, K., et al. 2018, A&A, 619, A135
Calzetti, D., Armus, L., Bohlin, R. C., et al. 2000, ApJ, 533, 682
Charlot, S. & Fall, S. M. 2000, ApJ, 539, 718
Cirasuolo, M., Afonso, J., Bender, R., et al. 2012, in SPIE Conference Series, Vol. 8446, Proc. SPIE, 84460S
Civano, F., Marchesi, S., Comastri, A., et al. 2016, ApJ, 819, 62
Corre, D., Buat, V., Basa, S., et al. 2018, A&A, 617, A141
Dickinson, M., Giavalisco, M., & GOODS Team. 2003, in The Mass of Galaxies at Low and High Redshift, ed. R. Bender & A. Renzini, 324
Elbaz, D., Dickinson, M., Hwang, H. S., et al. 2011, A&A, 533, A119
Guo, Y., Ferguson, H. C., Giavalisco, M., et al. 2013, ApJS, 207, 24
Kewley, L. J., Geller, M. J., & Jansen, R. A. 2004, AJ, 127, 2002
Khostovan, A. A., Sobral, D., Mobasher, B., et al. 2016, MNRAS, 463, 2363
Laigle, C., McCracken, H. J., Ilbert, O., et al. 2016, ApJS, 224, 24
Lutz, D., Poglitsch, A., Altieri, B., et al. 2011, A&A, 532, A90
Malek, K., Buat, V., Burgarella, D., et al. 2019, arXiv e-prints, arXiv:1904.12498
Maraston, C. & Strömbäck, G. 2011, MNRAS, 418, 2785
Marchesi, S., Civano, F., Elvis, M., et al. 2016, ApJ, 817, 34
Momcheva, I. G., Brammer, G. B., van Dokkum, P. G., et al. 2016, ApJS, 225, 27
Scoville, N., Aussel, H., Brusa, M., et al. 2007, ApJS, 172, 1
Steidel, C. C., Rudie, G. C., Strom, A. L., et al. 2014, ApJ, 795, 165
Suzuki, T. L., Kodama, T., Sobral, D., et al. 2016, MNRAS, 462, 181
Talia, M., Cimatti, A., Pozzetti, L., et al. 2015, A&A, 582, A80
Wang, T. in prep.